Journal of
Applied Crystallography

ISSN 0021-8898

Received 28 March 2013
Accepted 28 June 2013

Graphene as a protein crystal mounting material to reduce background scatter

Jennifer L. Wierman,[a] Jonathan S. Alden,[b] Chae Un Kim,[c] Paul L. McEuen[d,e,f] and Sol M. Gruner[c,d,e,f]*

[a]Field of Biophysics, Cornell University, Ithaca, NY 14853, USA, [b]School of Applied and Engineering Physics, Cornell University, Ithaca, NY 14853, USA, [c]Cornell High Energy Synchrotron Source (CHESS) and Macromolecular Diffraction Facility at CHESS (MacCHESS), Cornell University, Ithaca, NY 14853, USA, [d]Department of Physics, Cornell University, Ithaca, NY 14853, USA, [e]Kavli Institute at Cornell for Nanoscale Science, Cornell University, Ithaca, NY 14853, USA, and [f]Laboratory of Atomic and Solid State Physics, Cornell University, Ithaca, NY 14853, USA. Correspondence e-mail: smg26@cornell.edu,

The overall signal-to-noise ratio per unit dose for X-ray diffraction data from protein crystals can be improved by reducing the mass and density of all material surrounding the crystals. This article demonstrates a path towards the practical ultimate in background reduction by use of atomically thin graphene sheets as a crystal mounting platform for protein crystals. The results show the potential for graphene in protein crystallography and other cases where X-ray scatter from the mounting material must be reduced and specimen dehydration prevented, such as in coherent X-ray diffraction imaging of microscopic objects.

1. Introduction

Macromolecular crystallography is a foundational tool in structural biology. Limitations in crystallography arise from two distinct complications: radiation damage and the signal-to-noise ratio of diffraction data sets (Ravelli & Garman, 2006; Holton & Frankel, 2010). While radiation damage may be outrun with the application of an X-ray free-electron laser (Chapman *et al.*, 2011), or reduced by crystal cryocooling (Dewan & Tilton, 1987; Garman & Schneider, 1997; Haas & Rossmann, 1970; Hope, 1988; Low *et al.*, 1966), the signal-to-noise ratio is a multifaceted problem arising from everything in the path of the beam to the detector (Krieger *et al.*, 1974; Krieger & Stroud, 1976). In principle, all sources of background scatter except for disordered solvent internal to the crystal can be reduced by eliminating materials in the path of the X-ray beam.

Major sources of background scatter are the mounting materials that typically surround the crystal, such as external mother liquor, coating oil and enclosing capillaries (Kim *et al.*, 2013). Most of these materials are used to hold the crystal in the beam while staving off dehydration and/or protecting the crystal from the damaging effects of ice formation during cryocooling (Garman, 1999, 2003; Kwong & Liu, 1999; Riboldi-Tunnicliffe & Hilgenfeld, 1999; Garman & Doublié, 2003; Owen *et al.*, 2006; Haas & Rossmann, 1970; Hope, 1988; Henderson, 1990; Juers & Matthews, 2004). However, these responses to mounting, dehydration reduction and cryoprotection scatter X-rays which, for weakly diffracting crystals such as microcrystals, can hide the signal. The objective is to make the ordered protein crystal diffraction the most prominent source of X-rays seen by the detector. Thus, it is important to reduce the density and thickness of all matter in the beam external to the crystal.

Graphene is an attractive mounting material because it is composed of low atomic weight carbon and can be obtained in macroscopic sheets that are only a single atom thick yet remarkably strong (Neto & Novoselov, 2011; Lee *et al.*, 2011). Graphene is a planar layer of sp^2-bonded carbon atoms and has an attenuation length of 4988 μm for 13.5 keV X-rays. The thickness of each of these graphene layers is about 0.34 nm, so a few layers are essentially transparent to the X-rays used for crystallography.

Recent advances in the development of graphene membranes have allowed for 'easy' fabrication of sheets of carbon having the thickness of a single atomic layer (∼0.34 nm) using chemical vapor deposition (Li *et al.*, 2009). A single layer of graphene has been shown to be impermeable to standard gases, including helium at several atmospheres of pressure, in addition to being optically transparent (Bunch *et al.*, 2008; Yuk *et al.*, 2011). In recent studies, pockets of liquids containing crystals between layers of graphene have been used successfully even in the high-vacuum environment of transmission electron microscopy, resulting in improved image resolution and signal-to-noise ratios for acquired electron microscopy images (Yuk *et al.*, 2012; Mohanty *et al.*, 2011).

This study demonstrates the feasibility of graphene as a crystal mounting substrate. We show that graphene may be used to wrap and support protein crystals in both cryocooled and room-temperature crystallographic experiments. We employ five methods, which include both graphene-wrapped samples and samples mounted using more traditional methods. The graphene-wrapped sample preparations include

one method in which the sample is left at room temperature for over 10 min before flash-cooling, to show the robustness of the graphene covering for prevention of dehydration.

2. Materials and methods

2.1. Protein crystallization

Tetragonal crystals were prepared using the hanging-drop method (Ko *et al.*, 1994) with lyophilized thaumatin powder from *Thaumatococcus daniellii* (Sigma–Aldrich, St Louis, MO, USA). The powder was resuspended in deionized water to 25 mg ml^{-1} and 50 m*M* HEPES buffer at pH 7. The crystals were grown at 293 K in hanging drops comprising 2 µl of protein solution combined with 2 µl of a reservoir solution containing 0.9 *M* sodium potassium tartrate. The hanging drops were suspended, on a siliconized glass coverslip, over 800 µl wells of reservoir solution in a 24-well plate, and the assembly was sealed with vacuum grease. Small clear crystals appeared overnight and were incubated at room temperature for a few days until truncated bipyramidal crystals approximately 100 µm across were obtained. The crystals used in this study were almost identical in size for each method, with the size chosen to match the footprint of the beam. After unsealing, the hanging drops were mixed with glycerol to a final concentration of 0.9 *M* NaK tartrate with 10% glycerol for cryoprotection. Crystals were equilibrated for 1–2 min in this solution before being flash-cooled in liquid nitrogen, oil-coated and flash-cooled, or wrapped in graphene, as described below.

2.2. Oil-coating

In cases where a crystal was to be coated in oil as cryoprotection for comparison purposes, the hanging drop was covered directly with NVH oil (Hampton Research, Aliso Viejo, CA, USA) to prevent dehydration. The crystals were gently extracted from the mother liquor, and external mother liquor on the crystal was removed with gentle swishing so as to leave a tail of solvent behind with a cryoloop (Hampton Research). This was repeated until little-to-no solvent was left on the exterior of the crystal. The cryoloop was also used to extract the crystal from the oil droplet with as little external excess oil as possible and to hold the crystal during flash-cooling in liquid nitrogen.

2.3. Graphene chemical vapor deposition

Large-grain graphene was grown on copper foil (catalog No. 13382, Alfa Aesar, Ward Hill, MA, USA), by chemical-vapor deposition, using an enclosure method developed by Li *et al.* (2011). In this method, the copper growth foil is enclosed in a second copper foil, to limit exposure to growth gases, and placed in an evacuated furnace (base pressure 10^{-4} torr $\simeq$ 1.33×10^{-2} Pa). In a slight modification from the method of Li *et al.* (2011), the foil is annealed under flowing hydrogen at 60 standard cubic centimetres per minute (s.c.c.m.) at 1253 K for 45 min and then cooled to 1203 K. A flow of 3 s.c.c.m. of methane is added to the hydrogen, then the temperature is ramped to 1253 K over the course of an hour and held at 1253 K for 3 h, and finally the system is cooled to room temperature and the gases are turned off. The resulting graphene has 30–100 µm grains, with small $\sim$2 µm patches of bilayer at nucleation sites.

2.4. Graphene–polymer transfer

We spin 50–200 nm of poly(methyl methacrylate) (PMMA) onto one piece of the graphene-on-copper. After scratching the graphene off the back of the copper foil with steel wool, the copper is etched by floating it on the surface of an ammonium persulfate-based etchant (Transene APS 100). The PMMA-on-graphene is rinsed in multiple water baths and transferred to a second PMMA-free graphene-covered copper foil by scooping it out of the water using the foil and letting it dry. The copper is again etched, and the now two layers of graphene under PMMA are rinsed. This process is repeated until either three or five layers of graphene are stacked on top of each other underneath the PMMA. Finally, the PMMA-on-graphene is scooped out of the water using a piece of quartz wafer, and the drops of water are gently blown off using a nitrogen gun, while leaving a thin layer of water between the quartz and graphene. The wafer is then dipped in acetone and left for $\sim$3 min, during which time the PMMA dissolves and is mostly removed. It is gently lifted out of the acetone and slowly lowered back into the water, at which point the PMMA-free multilayer graphene lifts off the surface of the quartz (presumably as a result of the thin water layer still existing between the graphene and quartz) to float on the surface of the water. This process yields intact multilayer graphene on the centimetre scale, which can then be broken into smaller pieces and transferred to loops and other sample substrates.

2.5. Graphene preparation

The multilayer graphene was broken into smaller pieces of approximately 1 $\times$ 1 mm with tweezers while it rested on the surface of the water. These graphene pieces were then swept out in a suspension of deionized water with a small copper loop (5 mm in diameter), so that the multilayer graphene floated on the top of the water droplet within the copper loop. The entire copper loop was inverted so that the multilayer graphene 'floated' on the bottom of the suspended water droplet. The drop was then washed with protein crystallization reservoir solution several times, ensuring that the conditions within the suspended droplet were nearly identical to those for the crystallization hanging droplet for the protein crystals.

2.6. Graphene wrapping

Crystals were transferred *via* a pipette to the suspended drop in the copper loop containing the graphene sheet. The graphene floats at the water–air interface and can be visually located as a dark film with well defined edges compared to the solution around it. Crystals sank to the bottom of the drop by gravity and settled near the water–air interface. A cryoloop (Hampton Research, Aliso Viejo, CA, USA) was used to

carefully sweep the crystal to the center of the multilayer graphene piece using advection, being careful not to contact the crystal, as shown in Fig. 1(*a*). Once the crystal was properly seated on the multilayer graphene piece, the cryoloop was used to sandwich the crystal inside the multilayer graphene by sweeping the horizontal loop downward through the droplet, onto the multilayer graphene beside or around the crystal, and finally out of the bottom of the drop, as shown in Fig. 1(*b*). This causes the multilayer graphene to wrap around the crystal as the loop is pulled away from the larger droplet, and the surface tension draws the graphene around it. Fig. 2 shows two different crystals enclosed within three-layer and five-layer graphene sheets, for a total of either ∼6 layers or ∼10 layers of graphene in the path of the beam. In most samples, the graphene wraps closely around the crystal and suspends it within the cryoloop as in Fig. 2. Fig. 2(*c*) shows how the graphene creases within the loop from the contours of the crystal.

The following three post-treatments were applied to five-layer graphene-wrapped crystal samples:

(1) Samples were immediately flash-cooled and diffraction data collected [an example is shown in Fig. 3(*d*)].

(2) Samples were air dried for 10 min at room temperature before they were flash-cooled and diffraction data were collected (Fig. 3*e*).

(3) Diffraction data were obtained at room temperature, from samples that were allowed to remain in air at room temperature for approximately 5 min before data collection (Fig. 3*f*); the delay is due to the time needed to begin the diffraction experiment.

2.7. Crystallographic data collection and processing

Crystallographic X-ray diffraction data were collected at the Cornell High Energy Synchrotron Source (CHESS) at the F1 beamline station (λ = 0.9179 Å, *E* = 13.508 keV) using a 100 µm monochromatic X-ray beam from a 24-pole wiggler. For data collection, an Area Detector Systems Corporation (ADSC) Quantum 270 (Q270) detector was placed such that

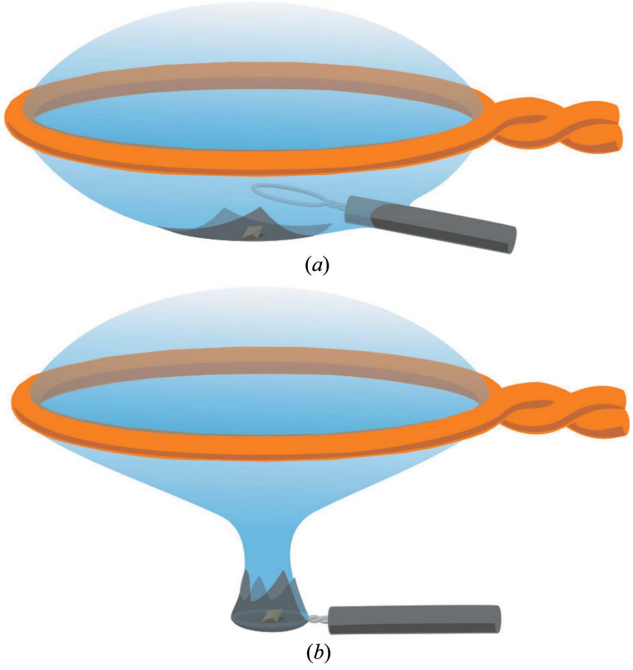

Figure 1
Graphic depicting how the graphene and crystal are mounted on a Hampton cryoloop. A copper loop supports a droplet of mother liquor solution. Graphene is floated on the bottom of the droplet, and a crystal is dropped in solution onto the hydrated side of the graphene. The cryoloop is then inserted into the droplet below the copper loop (*a*), oriented horizontally with the crystal situated in the center of the loop, and dragged out through the bottom of the solvent droplet (*b*). This causes the graphene to wrap around the crystal and the cryoloop.

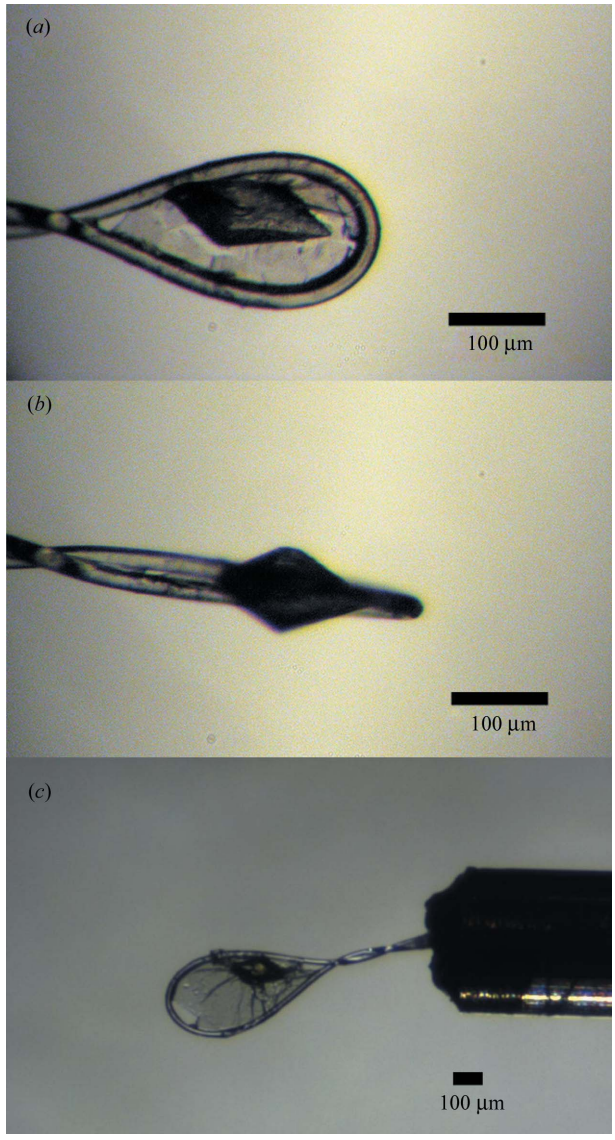

Figure 2
Cryocooled thaumatin crystals wrapped in graphene on a Hampton cryoloop. This figure shows two samples of crystals wrapped within graphene, supported in a cryoloop using the graphene as a scaffold. One sample wrapped in three layers of graphene is shown at orthogonal angles in (*a*) and (*b*), which illustrate the crystal placement within the cryoloop. (*c*) shows the crinkling and creasing of five-layer graphene along the contours of another crystal. All three images show the graphene completely covering the thaumatin crystals.

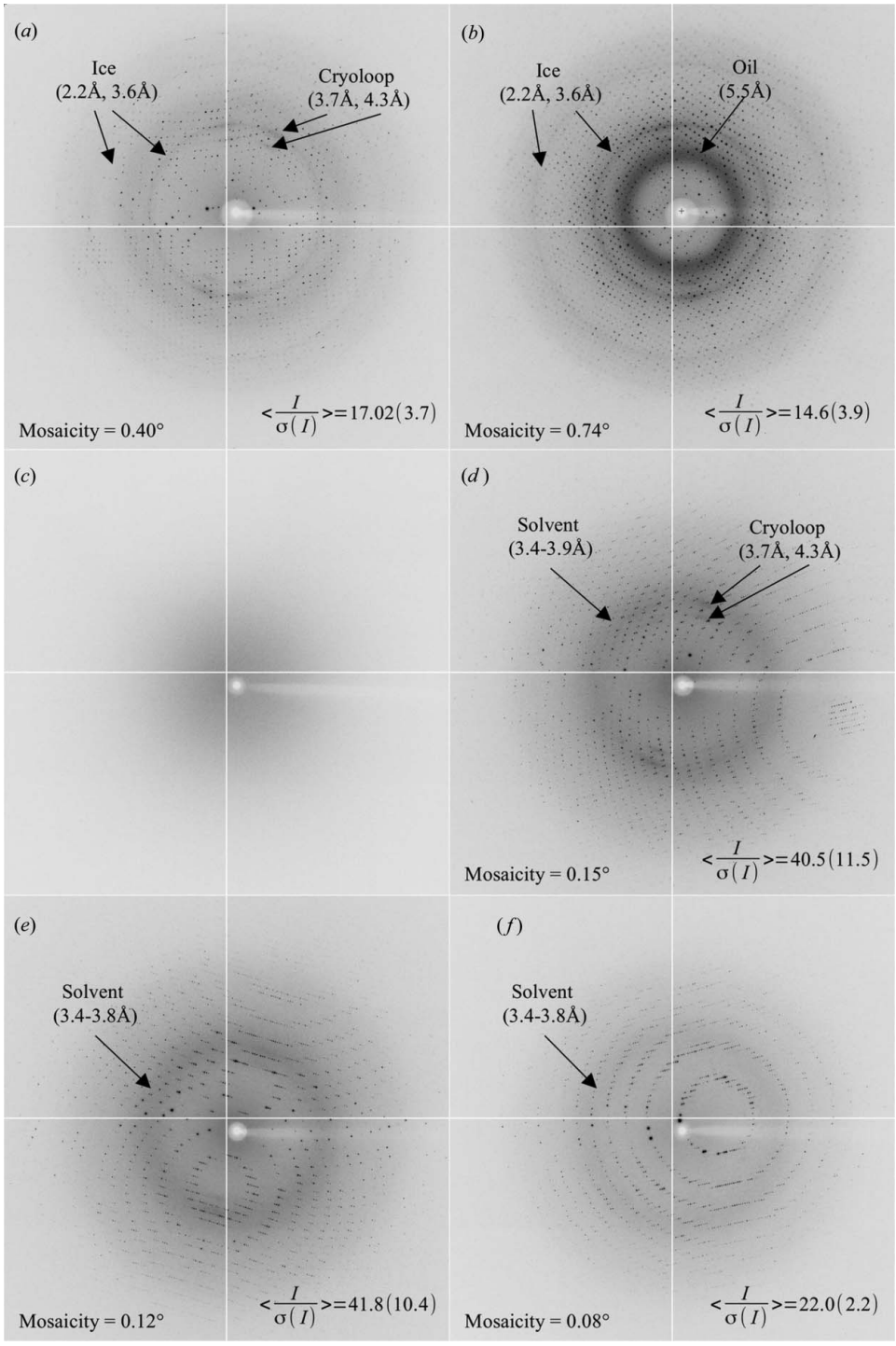

Figure 3
Diffraction patterns from five methods, including conventional and graphene-wrapped thaumatin crystals with 10% glycerol. (*a*) Diffraction from a crystal flash-cooled immediately after equilibration in crystal preparation. The faint ice rings (arrows) are due to the small amount of cryoprotectant used in the solvent. (*b*) Diffraction from a sample coated in oil to prevent dehydration and flash-cooled in liquid nitrogen before imaging. Again, there are faint ice rings due to the solvent's glycerol content. (*c*) Diffraction from a sample of graphene stretched across a cryoloop without crystals or solvent. The resultant scatter, which includes that from the graphene, is indistinguishable from the background scatter (data not shown). (*d*) Diffraction from a crystal wrapped in five-layer graphene and then directly flash-cooled in liquid nitrogen before diffraction. Note the absence of the ice rings, indicating that the amount of solution surrounding the crystal is small enough to eliminate the growth of ice crystals. (*e*) Diffraction from a crystal left at room temperature for 10 min after being wrapped in five-layer graphene, before being flash-cooled and exposed to X-rays. (*f*) Diffraction from a graphene-wrapped crystal diffracting at room temperature without any cooling.

the face was perpendicular to the beam, at a distance of 200 mm from the sample, corresponding to a largest inscribed circle of resolution of 1.4 Å. For each crystal sample, complete data sets were imaged at 100 K (or at ∼300 K for the room-temperature graphene-wrapped samples) with a 1° oscillation step size during each 1 s exposure, resulting in a 90° rotation overall. The software *HKL-2000* was used to index, refine, integrate and scale each 90° data set (Otwinowski & Minor, 1997). Parameters including unit-cell size, resolution, mosaicity, redundancy, completeness, $\langle I/\sigma(I)\rangle$ and $R_{\rm sym}$ were evaluated for every data set during the scaling process and compared between data sets.

Samples consisting of an 'empty' cryoloop and ten layers of graphene suspended across the cryoloop were also examined in order to determine the background scattering baseline arising from sources outside the crystal (air paths, collimator scatter *etc.*). No attempt was made to eliminate air scatter arising from the air path from the collimator to the beamstop.

3. Results

Tetragonal thaumatin crystals were determined to have a space group of $P4_12_12$ with a solvent content of 55–60% (*v*/*v*) calculated using the Matthews coefficient and the *CCP4* programming suite (Collaborative Computational Project, Number 4, 1994). Fig. 3 shows example diffraction images, at the same contrast level, taken from samples obtained using conventional methods of flash-cooling as well as those incorporating graphene. The diffraction images of crystals without graphene wrapping are shown in Figs. 3(*a*) and 3(*b*). The average mosaicity (of at least three crystals in each case) of the flash-cooled crystals (*e.g.* as in Fig. 3*a*) was 0.36° and $\langle I/\sigma(I)\rangle$ was 21.4,

Table 1
Data collection and processing statistics of thaumatin crystals.

A comparison of complete thaumatin diffraction data and statistics from three different methods of graphene-wrapped crystal mounting, along with standard graphene-free techniques. Values in parentheses are for the highest resolution shell. For room-temperature (RT) graphene-wrapped crystals, four data sets were analyzed. In the remaining four methods, three data sets each were analyzed.

Method†	Flash-cooled	Flash-cooled in oil	Graphene-wrapped (flash-cooled)	Graphene-wrapped (10 min delay at RT, flash-cooled)	Graphene-wrapped (RT)
Solvent condition	0.9 *M* NaK tartrate + 10% glycerol	0.9*M* NaK tartrate + 10% glycerol	0.9 *M* NaK tartrate + 10% glycerol	0.9 *M* NaK tartrate + 10% glycerol	0.9 *M* NaK tartrate + 10% glycerol
Space group	$P4_12_12$	$P4_12_12$	$P4_12_12$	$P4_12_12$	$P4_12_12$
Unit-cell parameters (Å)	$a = b = 58.25$, $c = 150.40$	$a = b = 58.62$, $c = 150.85$	$a = b = 57.80$, $c = 150.22$	$a = b = 57.80$, $c = 150.30$	$a = b = 58.70$, $c = 151.60$
Resolution range (Å)	50.0–1.60 (1.63–1.60)	50.0–1.60 (1.63–1.60)	50.0–1.60 (1.63–1.60)	50.0–1.60 (1.63–1.60)	50.0–1.60 (1.63–1.60)
No. of unique reflections	33845 (2034)	28021 (1431)	34506 (1675)	34650 (1679)	35967 (1769)
Redundancy	6.5 (5.8)	6.6 (4.7)	6.9 (5.3)	7.1 (6.7)	7.1 (6.6)
Completeness (%)	95.1 (100.0)	98.0 (80.6)	99.8 (100.0)	99.9 (99.9)	99.8 (99.8)
$R_{\rm sym}$ (%)‡	8.6 (33.3)	14.7 (15.2)	7.3 (30.4)	6.6 (20.5)	14.2 (87.2)
$\langle I/\sigma(I)\rangle$	17.0 (3.7)	14.6 (3.9)	40.5 (11.5)	41.8 (10.4)	22.0 (2.2)
Mosaicity (°)	0.40	0.74	0.15	0.12	0.08

† The data sets shown here were taken from the crystals whose respective diffraction images are shown in Figs. 3(*a*), 3(*b*) and 3(*d*)–3(*f*). The illuminated crystal volume was approximately the same in all cases. ‡ $R_{\rm sym} = \sum|I - \langle I\rangle|/\sum\langle I\rangle$.

whereas the oil-protected crystals (*e.g.* in Fig. 3*b*) had averages of 0.67° and 18.0, respectively. The 'empty' graphene cryoloop image (Fig. 3*c*) showed diffraction indistinguishable from background images with no loop and graphene mounted in the beam path (not shown). The scatter that is seen is primarily from air in the beam path.

Figs. 3 (*d*)–3(*f*) show representative diffraction images from crystals wrapped in graphene in three different conditions. Crystalline ice formation would result in ice rings corresponding to a spacing of around 3.65 Å: no such pattern was observed for any of the graphene-wrapped samples. There is also minimal diffuse scatter in all images from the solution, both around the crystals and in the inner solvent channels.

Fig. 3(*d*) shows the diffraction image of a crystal that was flash-cooled directly after being wrapped in five-layer graphene, *i.e.* there are five layers on either side of the crystal. Diffraction arcs from the nylon cryoloop are seen at spacings corresponding to about 3.7 and 4.3 Å. The crystal diffracts to 1.5 Å at the edge of the image and to about 1.4 Å at the corners. If the detector had been moved closer to the crystal, we believe that the crystal would have diffracted even further. A solvent ring at 3.4–3.9 Å is believed to arise primarily from solvent within the crystal.

A diffraction pattern from a graphene-wrapped thaumatin crystal that had been allowed to stand in air for 10 min prior to flash cryocooling is seen in Fig. 3(*e*). The diffraction is very similar to the case of immediate cryocooling (*e.g.* Fig. 3*d*). There are no sections of cryoloop present in the diffraction images, and the background scattering from solution in/around the crystal is even fainter. The image diffracts to the edge of the detector, which corresponds to 1.5 Å.

Lastly, Fig. 3(*f*) shows a diffraction image of a graphene-wrapped crystal that was not cryocooled and for which diffraction data were collected at room temperature. There is reduced background scatter, specifically from the resolution where water rings typically appear. However, the crystal diffracts to approximately 1.6 Å and does not diffract to the edges of the detector. This is believed to be due to the effect of radiation damage at room temperature.

Table 1 shows the diffraction data from representative data sets in each of the five experimental conditions. The second and third columns give results for comparison from thaumatin crystals not wrapped in graphene, but treated using the more conventional methods of flash-cooling with cryoprotectants without and with oil-coating, respectively. The fourth column shows results from a graphene-wrapped crystal cooled directly after mounting within the graphene in the cryoloop. The fifth column shows data from a graphene-wrapped crystal that was left to air dry after mounting in graphene in a cryoloop for 10 min before flash-cooling. The final column shows data from a graphene-wrapped crystal which was left at room temperature for the entire exposure set.

4. Discussion

Five layers of graphene wrapped around a thaumatin crystal produce background scatter indistinguishable from the background scatter in the absence of graphene. This agrees with expectations from a material only ten carbon atoms thick. The lifetimes of the graphene-wrapped cooled and room-temperature crystals were equivalent to those of crystals obtained using existing methods (Hope, 1988; Berger *et al.*, 2010; Kim *et al.*, 2013). There was no visual evidence of any effect from the physical contact of the graphene and the crystals.

4.1. Graphene-wrapped crystals give high-quality diffraction data sets without the need for external hydration

Complete data sets were acquired using the method of wrapping graphene around thaumatin crystals. This eliminates the need for external hydration methods involving enclosing

oils or capillaries. The results from graphene wrapping are comparable to those achieved using other methods of background reduction, such as high-pressure cryocooling with capillary shielding (Kim *et al.*, 2005, 2013). The graphene-wrapping technique gives reproducible results for thaumatin crystals. Graphene-wrapped crystals that were cryocooled diffracted to high resolution with mosaicities that were comparable to or better than those achieved with standard cryocooling procedures. The ease with which ice rings were eliminated is probably a consequence of the reduction in solvent external to the crystal. The absence of external coating material led to a reduction in background scatter and thus to an increase in the signal-to-noise ratio.

4.2. Graphene extends the time-dependent window for flash-cooling crystals during sample mounting and shows extension to room-temperature studies

Our study showed that a crystal could be handled in air for over 10 min after being wrapped in graphene but before being cryocooled, yet still remain hydrated well enough to yield superb diffraction results. These crystals showed no difference in diffraction quality compared to the samples immediately cryocooled in our study. This suggests that the graphene provides an environmental seal, thereby slowing evaporation and keeping the crystals hydrated for longer periods of time. In addition, the results show that crystals can diffract successfully at room temperature within graphene. Incidentally, the presence of graphene in place of surrounding materials with higher thermal mass, such as excess solvent or coating oil, facilitates a more successful cooling of the sample (Kim *et al.*, 2013). We believe this could lead to better results when cryocooling crystals.

4.3. The effects of quality and size suitable for crystallography

Electron microscopy (Yuk *et al.*, 2012; Mohanty *et al.*, 2011) and helium studies (Bunch *et al.*, 2008) prove that graphene can be vacuum tight, at least on nanometre-to-micrometre length scales. It is presently difficult to obtain larger sheets of monodomain graphene. However, graphene is the subject of intense study by many groups around the world, and the quality of the sheets being produced is constantly improving. High-quality sheets larger than a few tens of micrometres across are now routinely made in many laboratories. It is safe to predict that larger sheets will become available; in fact, some groups have produced some rare millimetre-size grains (Li *et al.*, 2011). In the meantime, this study shows that presently available multidomain multilayers are already good enough to mount crystals of the order of 100 μm across. We are confident that the same procedures will work with larger crystals.

5. Conclusion

In this study, we showed that the background scatter is greatly decreased by the addition of a graphene multilayer in place of external hydration methods. We have demonstrated the first incorporation of graphene in macromolecular crystallography, in order to increase the signal-to-noise ratio of diffraction patterns from protein crystals.

Graphene mounts may clearly be of importance in microcrystal diffraction. Holton & Frankel (2010) calculated that a micrometre-sized lysozyme crystal should yield a complete cryocooled data set to 2 Å resolution, provided that every diffracted X-ray is detected and there is no competing background scatter. Modern pixel array detectors can detect every X-ray with nearly 100% efficiency (Koerner *et al.*, 2011). Graphene can be used to effectively eliminate external background scatter: although no attempt was made to eliminate air scatter in the path length from the collimator to the main beamstop in this proof-of-principle study, one can readily extrapolate how this may be done. Electron microscopy (Yuk *et al.*, 2012) and helium gas studies (Bunch *et al.*, 2008) have already shown high-quality graphene sheets to be vacuum, water and helium gas tight on micrometre length scales. One can envision graphene-encased microcrystals held in a complete vacuum path environment where there is no main beam air scatter. In other cases where a microcrystal must be kept cryocooled, one can imagine a vacuum path that has a graphene vacuum window just short of a graphene-wrapped crystal held in a helium gas cryostream, followed by another graphene window into a vacuum path that encloses the beamstop and has a conventional vacuum window at the detector. Single-layer graphene windows tens of micrometres across have already been produced. Single- or multilayer graphene vacuum windows are feasible and are all that are needed for microcrystallography. In this case the total beam path in a cryocooled He gas stream can be reduced to very short lengths, *i.e.* smaller than a millimetre. The background scatter of such a system can be reduced to negligible levels relative to the diffraction from micrometre-sized crystals.

The results presented here have obvious extensions to preparation and mounting of many samples, not only for crystallography but for other techniques, ranging from X-ray scattering from weakly diffracting liquids and disordered materials, to sample mounts for objects in coherent X-ray diffraction imaging.

We thank Marian Szebenyi, Kate Green, David Schuller, Richard Gillilan, Irina Kriksunov, Bill Miller, Mike Cook and Scott Smith for their support. We thank Carlos Ruiz Vargas for helpful discussions regarding graphene transfer. This work is based upon research with support provided by the Molecular Biophysics Training grant T32GM008267 and conducted at CHESS, which is supported by the National Science Foundation (NSF) and the National Institutes of Health (NIH)/National Institute of General Medical Sciences under NSF award DMR0936384, using the Macromolecular Diffraction at CHESS (MacCHESS) facility, which is supported by NIH award GM103485. This work also was supported in part by the Air Force Office of Scientific Research (AFOSR) through the Graphene MURI and the NSF through the Cornell Center for

Materials Research (CCMR, NSF DMR0520404 and IMR0417392). Some sample fabrication was performed at the Cornell Nanoscale Science and Technology Facility, the Cornell node of the National Nanofabrication Infrastructure Network, funded by the NSF.

References

Berger, M. A., Decker, J. H. & Mathews, I. I. (2010). *J. Appl. Cryst.* **43**, 1513–1518.
Bunch, J. S., Verbridge, S. S., Alden, J. S., van der Zande, A. M., Parpia, J. M., Craighead, H. G. & McEuen, P. L. (2008). *Nano Lett.* **8**, 2458–2462.
Chapman, H. N. *et al.* (2011). *Nature*, **470**, 73–77.
Collaborative Computational Project, Number 4 (1994). *Acta Cryst.* D**50**, 760–763.
Dewan, J. C. & Tilton, R. F. (1987). *J. Appl. Cryst.* **20**, 130–132.
Garman, E. (1999). *Acta Cryst.* D**55**, 1641–1653.
Garman, E. F. (2003). *Curr. Opin. Struct. Biol.* **13**, 545–551.
Garman, E. F. & Doublié, S. (2003). *Methods Enzymol.* **368**, 188–216.
Garman, E. F. & Schneider, T. R. (1997). *J. Appl. Cryst.* **30**, 211–237.
Haas, D. J. & Rossmann, M. G. (1970). *Acta Cryst.* B**26**, 998–1004.
Henderson, R. (1990). *Proc. R. Soc. London Ser. B*, **241**, 6–8.
Holton, J. M. & Frankel, K. A. (2010). *Acta Cryst.* D**66**, 393–408.
Hope, H. (1988). *Acta Cryst.* B**44**, 22–26.
Juers, D. H. & Matthews, B. W. (2004). *Q. Rev. Biophys.* **37**, 105–119.
Kim, C. U., Kapfer, R. & Gruner, S. M. (2005). *Acta Cryst.* D**61**, 881–890.
Kim, C. U., Wierman, J. L., Gillilan, R., Lima, E. & Gruner, S. M. (2013). *J. Appl. Cryst.* **46**, 234–241.
Ko, T.-P., Day, J., Greenwood, A. & McPherson, A. (1994). *Acta Cryst.* D**50**, 813–825.
Koerner, L. J., Gillilan, R. E., Green, K. S., Wang, S. & Gruner, S. M. (2011). *J. Synchrotron Rad.* **18**, 148–156.
Krieger, M., Chambers, J. L., Christoph, G. G., Stroud, R. M. & Trus, B. L. (1974). *Acta Cryst.* A**30**, 740–748.
Krieger, M. & Stroud, R. M. (1976). *Acta Cryst.* A**32**, 653–656.
Kwong, P. D. & Liu, Y. (1999). *J. Appl. Cryst.* **32**, 102–105.
Lee, C., Wei, X., Kysar, J. W. & Hone, J. (2011). *Science*, **321**, 385–388.
Li, X. S., Cai, W. W., An, J. H., Kim, S., Nah, J., Yang, D. X., Piner, R. D., Velamakanni, A., Jung, I., Tutuc, E., Banerjee, S. K., Colombo, L. & Ruoff, R. S. (2009). *Science*, **324**, 1312–1314.
Li, X., Magnuson, C. W., Venugopal, A., Tromp, R. M., Hannon, J. B., Vogel, E. M., Colombo, L. & Ruoff, R. S. (2011). *J. Am. Chem. Soc.* **133**, 2816–2819.
Low, B. W., Chen, C. C. H., Berger, J. E., Singman, L. & Pletcher, J. F. (1966). *Proc. Natl Acad. Sci. USA*, **56**, 1746–1750.
Mohanty, N., Fahrenholtz, M., Nagaraja, A., Boyle, D. & Berry, V. (2011). *Nano Lett.* **11**, 1270–1275.
Neto, A. & Novoselov, K. (2011). *Rep. Prog. Phys.* **74**, 082501.
Otwinowski, Z. & Minor, W. (1997). *Methods Enzymol.* **276**, 307–326.
Owen, R. L., Rudiño-Piñera, E. & Garman, E. F. (2006). *Proc. Natl Acad. Sci. USA*, **103**, 4912–4917.
Ravelli, R. B. & Garman, E. F. (2006). *Curr. Opin. Struct. Biol.* **16**, 624–629.
Riboldi-Tunnicliffe, A. & Hilgenfeld, R. (1999). *J. Appl. Cryst.* **32**, 1003–1005.
Yuk, J. M., Kim, K., Aleman, B., Regan, W., Ryu, J. H., Park, J., Ercius, P., Lee, H. M., Alivisatos, A. P., Crommie, M. F., Lee, J. Y. & Zettl, A. (2011). *Nano Lett.* **11**, 3290–3294.
Yuk, J. M., Park, J., Ercius, P., Kim, K., Hellebusch, D. J., Crommie, M. F., Lee, J. Y., Zettl, A. & Alivisatos, A. P. (2012). *Science*, **336**, 61–64.